Physics Letters B 756 (2016) 153–160

Contents lists available at ScienceDirect

Physics Letters B

www.elsevier.com/locate/physletb

Measurement of the $e^+e^- \to K^+K^-\pi^+\pi^-$ cross section with the CMD-3 detector at the VEPP-2000 collider

D.N. Shemyakin [a,b,*], G.V. Fedotovich [a,b], R.R. Akhmetshin [a,b], A.N. Amirkhanov [a,b], A.V. Anisenkov [a,b], V.M. Aulchenko [a,b], V.Sh. Banzarov [a], N.S. Bashtovoy [a], A.E. Bondar [a,b], A.V. Bragin [a], S.I. Eidelman [a,b], D.A. Epifanov [a,e], L.B. Epshteyn [a,b,c], A.L. Erofeev [a,b], S.E. Gayazov [a,b], A.A. Grebenuk [a,b], S.S. Gribanov [a,b], D.N. Grigoriev [a,b,c], F.V. Ignatov [a,b], V.L. Ivanov [a,b], S.V. Karpov [a], V.F. Kazanin [a,b], I.A. Koop [a,b], A.A. Korobov [a,b], O.A. Kovalenko [a,b], A.N. Kozyrev [a,b], E.A. Kozyrev [a,b], P.P. Krokovny [a,b], A.E. Kuzmenko [a,b], A.S. Kuzmin [a,b], I.B. Logashenko [a,b], A.P. Lysenko [a], P.A. Lukin [a,b], K.Yu. Mikhailov [a,b], V.S. Okhapkin [a], Yu.N. Pestov [a], E.A. Perevedentsev [a,b], A.S. Popov [a,b], G.P. Razuvaev [a,b], Yu.A. Rogovsky [a,b], A.A. Ruban [a,b], N.M. Ryskulov [a], A.E. Ryzhenenkov [a,b], V.E. Shebalin [a,b], B.A. Shwartz [a,b], D.B. Shwartz [a,b], A.L. Sibidanov [a,d], Yu.M. Shatunov [a], E.P. Solodov [a,b], V.M. Titov [a], A.A. Talyshev [a,b], A.I. Vorobiov [a], Yu.V. Yudin [a,b], I.M. Zemlyansky [a]

[a] Budker Institute of Nuclear Physics, SB RAS, Novosibirsk, 630090, Russia
[b] Novosibirsk State University, Novosibirsk, 630090, Russia
[c] Novosibirsk State Technical University, Novosibirsk, 630092, Russia
[d] University of Sydney, School of Physics, Falkiner High Energy Physics, NSW 2006, Sydney, Australia
[e] University of Tokyo, Department of Physics, 7-3-1 Hongo Bunkyo-ku, Tokyo, 113-0033, Japan

ARTICLE INFO

Article history:
Received 5 October 2015
Received in revised form 20 February 2016
Accepted 29 February 2016
Available online 4 March 2016
Editor: M. Doser

ABSTRACT

The process $e^+e^- \to K^+K^-\pi^+\pi^-$ has been studied in the center-of-mass energy range from 1500 to 2000 MeV using a data sample of 23 pb^{-1} collected with the CMD-3 detector at the VEPP-2000 e^+e^- collider. Using about 24 000 selected events, the $e^+e^- \to K^+K^-\pi^+\pi^-$ cross section has been measured with a systematic uncertainty decreasing from 11.7% at 1500–1600 MeV to 6.1% above 1800 MeV. A preliminary study of $K^+K^-\pi^+\pi^-$ production dynamics has been performed.

1. Introduction

A high-precision measurement of the total cross section of $e^+e^- \to$ *hadrons* is important for various applications including a calculation of the hadronic contribution to the muon anomalous magnetic moment $(g-2)_\mu$ in the frame of the Standard Model. To confirm the existing difference between the calculated $(g-2)_\mu$ value [1] and the measured one [2], new measurements of the exclusive channels of $e^+e^- \to$ *hadrons* with better accuracy are required. A contribution to the muon anomalous magnetic moment from $e^+e^- \to K\bar{K}\pi\pi$ at the center-of-mass (c.m.) energies below 2 GeV is $(3.31 \pm 0.58) \times 10^{-10}$, estimated using isospin relations [1]. However, this result strongly depends on assumptions made about the presence of intermediate resonances, necessitating therefore a thorough study of the process dynamics in various $K\bar{K}\pi\pi$ final states ($K^+K^-\pi^+\pi^-$, $K^+K^-\pi^0\pi^0$, $K^\pm K^0_{S(L)}\pi^\mp\pi^0$, ...).

The process $e^+e^- \to K^+K^-\pi^+\pi^-$ has been earlier studied with the DM1 [3] and DM2 [4] detectors and more recently with much larger effective integrated luminosity at the BaBar [5,6] and Belle [7] detectors using an ISR approach. The first study of the production dynamics with the BaBar detector exhibited a plethora of the resonant substructures ($K^+K^-\rho$, $K^*K\pi$, $\phi\pi^+\pi^-$, K_1K, etc.) and some of them have been studied in more detail [6].

* Corresponding author at: Budker Institute of Nuclear Physics, SB RAS, Novosibirsk, 630090, Russia.
E-mail address: dimnsh@yandex.ru (D.N. Shemyakin).

http://dx.doi.org/10.1016/j.physletb.2016.02.072

In this paper we report a measurement of the $e^+e^- \to K^+K^-\pi^+\pi^-$ cross section and a preliminary study of production dynamics based on 23 pb^{-1} of an integrated luminosity collected by scanning of the c.m. energy ($E_{\text{c.m.}}$) range from 1500 to 2000 MeV.

2. Detector and data set

The VEPP-2000 electron–positron collider [8] at Budker Institute of Nuclear Physics (Novosibirsk, Russia) covers a c.m. energy range from 320 to 2000 MeV and employs a novel technique of round beams to reach luminosity up to 10^{32} cm^{-2} s^{-1} at $E_{\text{c.m.}} = 2000$ MeV. The Cryogenic Magnetic Detector (CMD-3) described in [9] is installed in one of the two beam interaction regions. The detector tracking system consists of the cylindrical drift chamber (DC) and double-layer cylindrical multiwire proportional Z-chamber, both also are used for a trigger and installed inside a thin (0.085 X_0) superconducting solenoid with 1.3 T magnetic field. DC contains 1218 hexagonal cells in 18 layers and allows one to measure charged particle momentum with 1.5–4.5% accuracy in the (100–1000) MeV/c range, and the polar (θ) and azimuthal (ϕ) angles with 20 mrad and 3.5–8.0 mrad accuracy, respectively. Amplitude information from the DC wires is used to measure the ionization losses (dE/dx_{DC}) of charged particles with $\sigma_{dE/dx_{\text{DC}}} = 11$–$14\%$ accuracy. The barrel electromagnetic calorimeters based on liquid xenon (LXe) (5.4 X_0) and CsI crystals (8.1 X_0) are placed outside the solenoid [10]. The total amount of material in front of the calorimeter is 0.13 X_0 that includes the solenoid as well as the radiation shield and vacuum vessel walls. BGO crystals (13.4 X_0) are used as the endcap calorimeter. The flux return yoke is surrounded by scintillation counters which are used to tag cosmic events.

To study a detector response and determine a detection efficiency, we have developed a code for Monte Carlo (MC) simulation of our detector based on the GEANT4 [11] package so that all simulated events are subjected to the same reconstruction and selection procedures as applied to the data. MC simulation of the signal process described further in Section 4 includes photon radiation by an initial electron or positron calculated according to [12].

For the present analysis we use data of 2011 (1.0 T field) and 2012 (1.3 T field) runs, collected at 66 beam energy points with 35 pb^{-1} of an integrated luminosity. In the 2011 run the energy range ($E_{\text{c.m.}} = 1000$–2000 MeV) was scanned up and down with a 25 MeV step collecting about 500 nb^{-1} per point. In the 2012 run this range was scanned up with 20–40 MeV steps collecting about 1 pb^{-1} per point. The integrated luminosity was determined using events of the processes $e^+e^- \to e^+e^-$ and $e^+e^- \to \gamma\gamma$ with about 1% accuracy [13].

The beam energy was monitored by measuring the current in the dipole magnets of the main ring, and, in addition, at a few energy points by using the Back-Scattering-Laser-Light system [14,15]. Using the measured average momentum value of Bhabha events and the average momentum of proton–antiproton pairs from the process $e^+e^- \to p\bar{p}$ [16], we determined $E_{\text{c.m.}}$ for each energy point with about 6 MeV and 2 MeV accuracy for 2011 and 2012 runs, respectively.

3. Events selection

Candidates for the events of the process under study are required to have three or four "good" tracks in the DC with the following "good" track definition:

- A track produces more than nine hits in the DC.
- A track momentum is larger than 50 MeV/c.

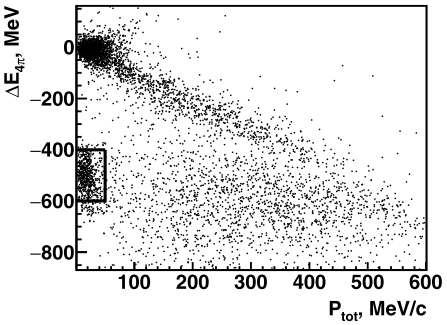

Fig. 1. Scatter plot of the $\Delta E_{4\pi}$ vs the total momentum P_{tot} for four-track events at $E_{\text{c.m.}} = 1980$ MeV.

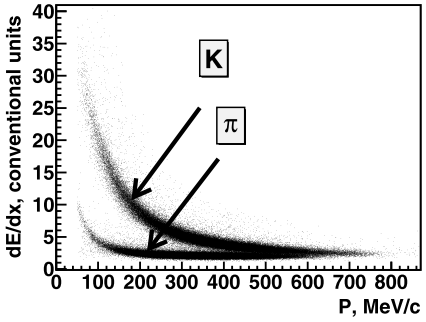

Fig. 2. The ionization losses in DC vs particle momentum for four-track events in simulation of signal process.

- A minimum distance from the track to the beam axis in the transverse plane is less than 0.4 cm.
- A distance from the track to the center of the interaction region along the beam axis is less than 10 cm.
- A polar angle of the track is in the range from 0.85 to $\pi - 0.85$ radians.
- Ionization losses of the track are less than ionization losses of the proton.

For selected events with four "good" tracks we calculate the total momentum P_{tot} and the total energy $E_{4\pi}$, assuming all particles to be pions:

$$P_{\text{tot}} = |\sum_{i=1}^{4} \vec{p}_i|, \qquad E_{4\pi} = \sum_{i=1}^{4} \sqrt{p_i^2 + m_\pi^2}\,.$$

Fig. 1 shows a scatter plot of the difference $\Delta E_{4\pi} = E_{4\pi} - E_{\text{c.m.}}$ vs the total momentum P_{tot}. The $e^+e^- \to \pi^+\pi^-\pi^+\pi^-$ events locate near the origin of the coordinates. Another cluster of events with a close to zero total momentum but shifted down along the vertical axis corresponds to $K^+K^-\pi^+\pi^-$ events. Events with high P_{tot} have missing particles and correspond to various background processes: $e^+e^- \to \pi^+\pi^-\pi^+\pi^-(\gamma)$, $K^0_S K^\pm\pi^\mp(\gamma)$, $\pi^+\pi^-\pi^+\pi^-\pi^0(\gamma)$, $\pi^+\pi^-\pi^+\pi^-\pi^0\pi^0(\gamma)$, $\pi^+\pi^-\pi^+\pi^-\pi^+\pi^-(\gamma)$.

Using the selections $P_{\text{tot}} < 50$ MeV/c and $|\Delta E_{4\pi} + 500| < 100$ MeV we obtain a sample of $K^+K^-\pi^+\pi^-$ events with a contribution from the background processes of less than 5% estimated according to simulation. These events are used to develop a procedure of separation of pions and kaons.

K/π separation in CMD-3 can be performed by analyzing ionization losses in the DC and the LXe calorimeter. The ionization losses dE/dx_{DC} in the DC for kaons and pions from simulated $K^+K^-\pi^+\pi^-$ events are shown in Fig. 2. A similar plot for the ionization losses dE/dx_{LXe} in the LXe calorimeter is shown in Fig. 3.

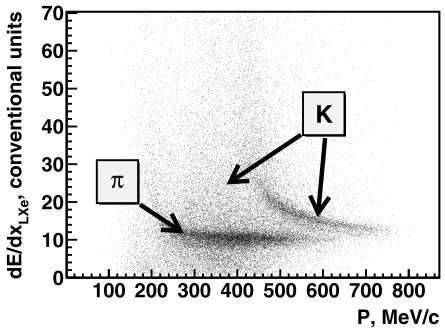

Fig. 3. Ionization losses in the LXe calorimeter vs momentum for $K^+K^-\pi^+\pi^-$ events in simulation.

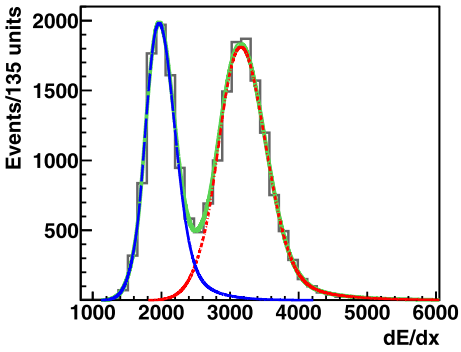

Fig. 4. Ionization losses for tracks with momentum in the 470–520 MeV/c range. The lines show PDFs for pions and kaons, described in the text.

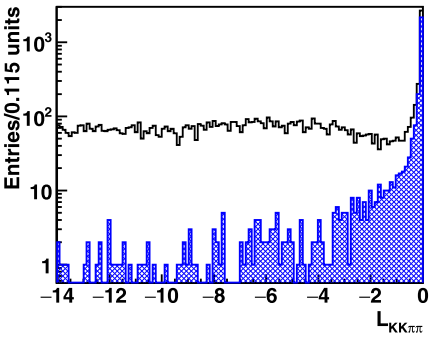

Fig. 5. Distribution of the likelihood function $L_{KK\pi\pi}$ for all three- and four-track events in data (open histogram), and for $K^+K^-\pi^+\pi^-$ simulated events (hatched histogram).

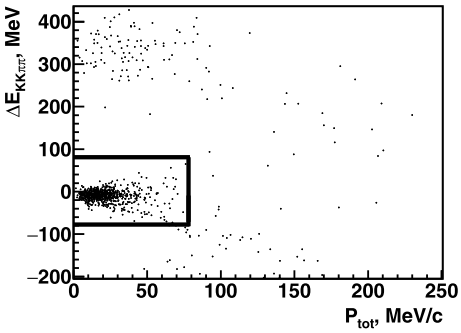

Fig. 6. The scatter plot of the difference $\Delta E_{KK\pi\pi}$ between the total energy and c.m. energy vs the total momentum for the four-track events at $E_{\text{c.m.}} = 1980$ MeV. The rectangle shows the selected area.

It can be seen that dE/dx_{DC} differ significantly for kaons and pions for momenta less than 500 MeV/c, while dE/dx_{LXe} differ even at higher momenta, so one can perform K/π separation in the whole particle momentum range. The distributions of the ionization losses have different shapes in the DC and the LXe calorimeter. It is Gaussian for dE/dx_{DC}, while nuclear interactions are likely in the LXe calorimeter, resulting in the wide tails of the dE/dx_{LXe} distribution, in which about 20% of the events are located. Simulation of nuclear interactions of kaons and pions in LXe is not perfect, especially at low momenta, so using simulated dE/dx_{LXe} results in uncontrollable systematic uncertainties. Thus an experimental input is required for studying energy deposition of particles in the LXe calorimeter and ionization losses in the drift chamber are only used in this analysis. This results in a less than 0.5% uncertainty in K/π separation estimated from simulation, where the particle type and the number of misidentified particles are known. This uncertainty is negligible compared to the total systematic error (discussed in Section 7).

We use momentum and dE/dx_{DC} values for each track to construct probability density functions (PDF) for kaons $f_K(p, dE/dx_{\text{DC}})$ and pions $f_\pi(p, dE/dx_{\text{DC}})$, each of which is a sum of Gaussian and logarithmic Gaussian distributions. The parameters of PDF are determined by approximating the dE/dx_{DC} histogram by PDF. The parameters of these functions are fitted by smooth lines which depend on momentum. First we use a sample of $e^+e^- \to \pi^+\pi^-\pi^+\pi^-$ events to determine $f_\pi(p, dE/dx_{\text{DC}})$, then the function $f_K(p, dE/dx_{\text{DC}})$ is determined using $e^+e^- \to K^+K^-\pi^+\pi^-$ events. The control sample of $e^+e^- \to \pi^+\pi^-\pi^+\pi^-$ events is selected using strong cuts, that reject the background to the level of less than 0.5%. The background in the sample of $e^+e^- \to K^+K^-\pi^+\pi^-$ events is about 1% and will be discussed below in this section. This procedure is performed separately for simulation and experiment. The approximation of the simulated dE/dx_{DC} distribution with a sum of two functions $f_K(p, dE/dx_{\text{DC}})$ and $f_\pi(p, dE/dx_{\text{DC}})$ in the momentum range 470–520 MeV/c is presented in Fig. 4.

Selection of events of the process $e^+e^- \to K^+K^-\pi^+\pi^-$ from the three- and four-track samples is performed using a likelihood function $L_{KK\pi\pi}$, which is constructed as:

$$L_{KK\pi\pi} = \ln\left(\frac{\prod f^i_\alpha(p, dE/dx_{\text{DC}})}{\prod[f^i_\pi(p, dE/dx_{\text{DC}}) + f^i_K(p, dE/dx_{\text{DC}})]}\right),$$

where i — track index, which varies from 1 to 3 or 4, $\alpha_i = K, \pi$ — assumed type of a particle corresponding to the i-th track. Under the assumption that each event is from the process $e^+e^- \to K^+K^-\pi^+\pi^-$, two tracks with opposite charges should be identified as kaons while the other two as pions and we test all possible combinations of α_i to obtain the maximum value of $L_{KK\pi\pi}$.

Fig. 5 shows the $L_{KK\pi\pi}$ value for all three- and four-track events in data by the open histogram, while the hatched histogram corresponds to the $K^+K^-\pi^+\pi^-$ events from simulation. The likelihood function value is a good parameter for separating $K^+K^-\pi^+\pi^-$ events from the background. We applied a requirement $L_{KK\pi\pi} > -3$ which retains more than 95% of signal events.

We assign pion or kaon mass to each track and calculate total energy $E_{KK\pi\pi}$. Fig. 6 shows a scatter plot of the difference $\Delta E_{KK\pi\pi} = E_{KK\pi\pi} - E_{\text{c.m.}}$ vs the total momentum for events with four tracks assuming all events to be $e^+e^- \to K^+K^-\pi^+\pi^-$, and the condition $L_{KK\pi\pi} > -3$ applied. Events of the process $e^+e^- \to K^+K^-\pi^+\pi^-$ are located near the origin of the coordinates.

The width of the $E_{KK\pi\pi}$ distribution for $K^+K^-\pi^+\pi^-$ events is a few times smaller than that of the $E_{4\pi}$ distribution while the shapes of the background distribution are the same for

Table 1
Center-of-mass energy, integrated luminosity, number of four-track events, number of three-track events, detection efficiency, radiative correction and Born cross section of the process $e^+e^- \to K^+K^-\pi^+\pi^-$. Errors are statistical only.

$E_{c.m.}$, MeV	Lum., nb^{-1}	N_4	N_3	ϵ	$(1+\delta)$	σ, nb
2004.6±6	478.1	313	380.5	0.390	0.972	3.88 ± 0.15
1988.6±2	600.6	445	507.7	0.410	0.956	4.10 ± 0.13
1978.4±6	506.6	353	412.0	0.398	0.949	4.05 ± 0.15
1966.9±2	692.2	510	650.6	0.416	0.942	4.35 ± 0.13
1952.6±6	451.0	326	390.0	0.407	0.937	4.23 ± 0.16
1944.8±2	993.8	735	898.9	0.422	0.935	4.23 ± 0.10
1927.0±6	590.8	441	532.2	0.413	0.933	4.35 ± 0.14
1926.0±6	566.9	420	569.1	0.426	0.933	4.47 ± 0.14
1903.2±2	900.4	682	841.0	0.431	0.930	4.31 ± 0.11
1901.3±6	498.6	351	471.0	0.418	0.930	4.33 ± 0.15
1893.4±6	527.1	381	459.1	0.420	0.928	4.17 ± 0.14
1874.2±2	855.6	659	723.0	0.436	0.919	4.09 ± 0.11
1871.1±6	671.0	497	658.3	0.424	0.917	4.50 ± 0.13
1848.6±6	435.4	311	395.8	0.429	0.903	4.27 ± 0.16
1840.0±2	966.0	721	1007.6	0.438	0.897	4.63 ± 0.11
1826.4±6	513.8	383	463.0	0.429	0.889	4.38 ± 0.15
1798.0±2	998.4	684	865.4	0.436	0.875	4.14 ± 0.11
1792.9±6	449.1	289	388.6	0.428	0.873	4.11 ± 0.16
1773.7±6	560.6	297	396.9	0.425	0.867	3.43 ± 0.13
1757.7±2	971.9	459	635.5	0.431	0.864	3.08 ± 0.09
1741.6±6	542.3	208	269.9	0.422	0.863	2.47 ± 0.11
1723.1±6	530.7	185	235.0	0.423	0.863	2.20 ± 0.11
1715.8±2	812.1	257	398.8	0.428	0.862	2.24 ± 0.09
1692.8±6	494.2	132	166.6	0.421	0.850	1.73 ± 0.10
1674.1±2	894.7	220	273.5	0.415	0.835	1.64 ± 0.07
1669.4±6	572.2	111	168.1	0.409	0.832	1.45 ± 0.09
1643.0±6	462.7	72	62.9	0.393	0.821	0.87 ± 0.08
1622.9±6	517.8	31	52.6	0.378	0.824	0.52 ± 0.06
1595.0±2	832.7	39	35.8	0.356	0.827	0.29 ± 0.03
1593.8±6	449.8	16	35.2	0.354	0.827	0.39 ± 0.06
1571.9±6	522.0	7	–	0.136	0.825	0.119 ± 0.045
1543.2±6	512.0	3	–	0.128	0.823	0.056 ± 0.032
1522.4±6	539.5	1	–	0.121	0.821	0.019 ± 0.019
1514.6±2	847.4	3	–	0.121	0.821	0.036 ± 0.020
1494.1±6	556.8	1	–	0.120	0.819	0.018 ± 0.018
1434.9±6	927.3	2	–	0.120	0.815	0.022 ± 0.016

$E_{4\pi}$ and $E_{KK\pi\pi}$. For that reason, conditions on $\Delta E_{KK\pi\pi}$ and $P_{\rm tot}$ allow to suppress the $e^+e^- \to \pi^+\pi^-\pi^+\pi^-(\gamma)$ background. However, five- and six-body processes with a missing particle in the final state ($\pi^+\pi^-\pi^+\pi^-\pi^0(\gamma)$, $\pi^+\pi^-\pi^+\pi^-\pi^0\pi^0(\gamma)$, $\pi^+\pi^-\pi^+\pi^-\pi^+\pi^-(\gamma)$), or four-body processes with charged kaons ($K^0_S K^\pm\pi^\mp(\gamma)$ at c.m. energy less than 2 GeV) have the same value of $E_{KK\pi\pi}$ and $P_{\rm tot}$ as the signal process. The condition on $L_{KK\pi\pi}$ allows one to significantly reduce the number of such background events. Application of the requirements $|\Delta E_{KK\pi\pi}| < 80$ MeV, $P_{\rm tot} < 80$ MeV/c and $L_{KK\pi\pi} > -3$ decreased the background to less than 1% level as estimated using the multihadron Monte Carlo generator [17]. In this generator all experimentally measured processes of e^+e^- annihilation into hadrons up to 2 GeV are used to calculate a total cross section at a given c.m. energy and events of each final state are sampled with a probability proportional to the fraction of its measured cross section in the total one.

The $L_{KK\pi\pi} > -3$ requirement for the three-track events selects candidates for the $K^+K^-\pi^+\pi^-$ final state for which we know the charge and type of a missing particle. Using the total momentum of three detected tracks and momentum conservation, we calculate the energy of the missing particle and add it to the energy of the detected particles to obtain the total energy E_{3+1} for these events. The histogram in Fig. 7 shows the difference between the calculated total energy for events with one missing particle and the c.m. energy, $\Delta E_{3+1} = E_{3+1} - E_{\rm c.m.}$. To extract the yield of signal events, we fit this distribution with a signal function and a linear background. The signal function shape is obtained using four-track $K^+K^-\pi^+\pi^-$ events assuming that one track is not detected. According to simulation [17], the linear function describes the background well.

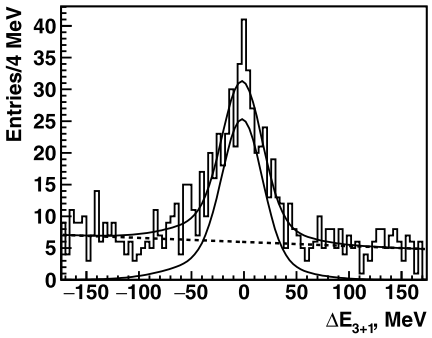

Fig. 7. Difference ΔE_{3+1} between the calculated total energy for events with one missing particle and the c.m. energy at $E_{\rm c.m.} = 1980$ MeV. The lines show a fit explained in the text.

Events with a missing particle mainly appear due to the limited DC acceptance, in addition, some tracks are not reconstructed due to a DC inefficiency, decays in flight or nuclear interaction.

Using distributions of ΔE_{3+1} parameter we determine separately the number of missing pions or kaons expected inside and outside the DC acceptance. Events with a missing track are used to study a reconstruction efficiency as discussed in Section 5.

In total, 10 545 four-track and 13 349 three-track events of the process $e^+e^- \to K^+K^-\pi^+\pi^-$ have been selected. The numbers of signal events at each energy point are listed in Table 1.

4. Simulation

A MC generator of the process $e^+e^- \to K^+K^-\pi^+\pi^-$ has been developed to obtain a detector response to $K^+K^-\pi^+\pi^-$ events and to calculate the detection efficiency. Since the DC acceptance is only 70% of the total solid angle, the correct determination of the total detection efficiency requires adequate simulation of the production dynamics of $e^+e^- \to K^+K^-\pi^+\pi^-$ events. The BaBar Collaboration reported observation of the following intermediate states for this process [6]: $\phi(1020)f_0(980)$, $\phi(1020)f_0(500)$, $K_1(1270,1400)K$, $K^*(892)^0K\pi$, $K_2^*(1430)^0K$ and $\rho(770)K^+K^-$. Following this study, we developed a MC generator which includes various processes resulting in the $K\bar{K}\pi\pi$ final state:

- $e^+e^- \to K^*(892)^0K\pi + c.c.$
- $e^+e^- \to K^*(892)^0\bar{K}^*(892)^0$
- $e^+e^- \to f_0(980)\phi$
- $e^+e^- \to f_0(500)\phi$
- $e^+e^- \to \rho(KK)_{\text{S-wave}}$
- $e^+e^- \to (K_1(1270)K)_{\text{S-wave}} \to (K^*\pi)_{\text{S-wave}}K$
- $e^+e^- \to (K_1(1400)K)_{\text{S-wave}} \to (K^*\pi)_{\text{S-wave}}K$
- $e^+e^- \to (K_1(1270)K)_{\text{S-wave}} \to (\rho K)_{\text{S-wave}}K$

The matrix element $M(\vec{p}_{K^+}, \vec{p}_{K^-}, \vec{p}_{\pi^-}, \vec{p}_{\pi^+}, \vec{\alpha})$ is written as a weighted sum of the amplitudes of all intermediate states mentioned above with the relative phases assumed to be 0° or 180°. The propagators of the intermediate resonances include relevant energy dependence of the width. The weights of the intermediate-state amplitudes are obtained from a minimization of the likelihood function

$$L(\vec{\alpha}) = \prod_i \frac{P^i_{\text{det}}(\vec{\alpha})}{Z(\vec{\alpha})},$$

where multiplication is performed for experimental events, $P_{\text{det}}(\vec{\alpha})$ – the probability to detect an $e^+e^- \to K^+K^-\pi^+\pi^-$ event, $\vec{\alpha}$ is the vector of the weights – free parameters of the fit, $Z(\vec{\alpha})$ – normalization coefficient. The probability to detect an $e^+e^- \to K^+K^-\pi^+\pi^-$ event with particle momenta $(\vec{p}_{K^+}, \vec{p}_{K^-}, \vec{p}_{\pi^-}, \vec{p}_{\pi^+})$ is defined as:

$$P^i_{\text{det}} = |M(\vec{p}^{\,i}_{K^+}, \vec{p}^{\,i}_{K^-}, \vec{p}^{\,i}_{\pi^-}, \vec{p}^{\,i}_{\pi^+}, \vec{\alpha})|^2 \times \epsilon(\vec{p}^{\,i}_{K^+}, \vec{p}^{\,i}_{K^-}, \vec{p}^{\,i}_{\pi^-}, \vec{p}^{\,i}_{\pi^+})\Delta F^i,$$

where $\epsilon(\vec{p}^{\,i}_{K^+}, \vec{p}^{\,i}_{K^-}, \vec{p}^{\,i}_{\pi^-}, \vec{p}^{\,i}_{\pi^+})$ – detection efficiency, ΔF – element of the event phase space. The calculation of

$$Z(\vec{\alpha}) = \frac{\int |M(\vec{p}_{K^+}, \vec{p}_{K^-}, \vec{p}_{\pi^-}, \vec{p}_{\pi^+}, \vec{\alpha})|^2 \epsilon(\vec{p}_{K^+}, \vec{p}_{K^-}, \vec{p}_{\pi^-}, \vec{p}_{\pi^+}) dF}{N_{\text{event}}},$$

where N_{event} – the total number of events, is performed using MC simulation. It can be seen that

$$L \propto \prod_i \frac{|M(\vec{p}^{\,i}_{K^+}, \vec{p}^{\,i}_{K^-}, \vec{p}^{\,i}_{\pi^-}, \vec{p}^{\,i}_{\pi^+}, \vec{\alpha})|^2}{Z(\vec{\alpha})}$$

for a fixed sample of events, because the factor $\prod_i \epsilon(\vec{p}^{\,i}_{K^+}, \vec{p}^{\,i}_{K^-}, \vec{p}^{\,i}_{\pi^-}, \vec{p}^{\,i}_{\pi^+})\Delta F^i$ is independent of $\vec{\alpha}$. The last equation for L was used in minimization.

Since the number of events at each c.m. energy point is not sufficient to determine the weights, the events are combined into nine groups with the following average values of $E_{\text{c.m.}}$: 1600, 1650, 1700, 1750, 1800, 1850, 1900, 1950 and 2000 MeV.

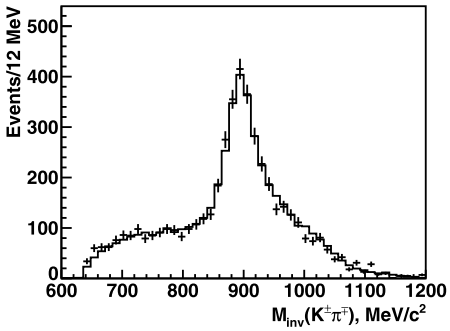

Fig. 8. $K^\pm\pi^\mp$ invariant mass for data (points) and MC simulation (histogram) at $E_{\text{c.m.}} = 1950$ MeV.

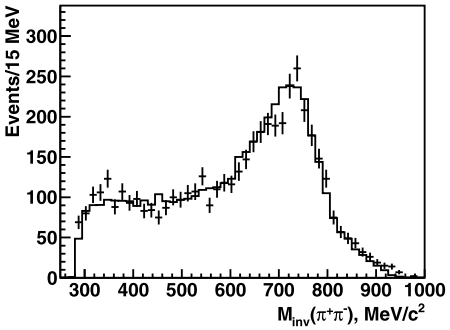

Fig. 9. $\pi^+\pi^-$ invariant mass for data (points) and MC simulation (histogram) at $E_{\text{c.m.}} = 1950$ MeV.

We found no significant contribution from the $K^*(892)^0K\pi$ and $K^*(892)^0\bar{K}^*(892)^0$ channels and excluded them from L. We observe strong dependence of the weights of the intermediate-state amplitudes on the c.m. energy and high interference between various amplitudes. It was found that the main intermediate mechanisms are $e^+e^- \to (K_1(1270,1400)K)_{\text{S-wave}} \to (K^*\pi)_{\text{S-wave}}K$, their contribution is about 50–90% and depends on c.m. energy. The $K_1(1270)$ and $K_1(1400)$ are broad resonances and phase space of the K_1K system is small at energies smaller than 2 GeV. So a much larger sample is needed for separation of the intermediate states with these particles.

The dependence of the weights of the intermediate-state amplitudes on the c.m. energy has been smoothed and then used to construct a MC generator that was used for the final detection efficiency calculation. The obtained contributions of various intermediate states are consistent with the BaBar results. A detailed analysis of the production dynamics will be performed after increasing statistics and a study of the other charge combinations of the $K\bar{K}\pi\pi$ final state.

Comparison of simulated and experimental invariant mass and angular distributions for the c.m. energy of 1950 MeV is shown in Figs. 8–13. The points with error bars correspond to experimental data, the histograms correspond to simulation; the obtained mixture of the intermediate states reasonably describes the data.

5. Efficiency

We calculate the detection efficiency from simulation as a ratio of the number of events after the selections described in Sec. 3 and the total number of simulated events. Fig. 14 shows the detection efficiency calculated in our model for four-track events (circles), events with a missing pion (stars), events with a missing kaon (squares), and the total one (triangles) vs c.m. energy. The detection efficiency calculated in our model is 10% smaller than that in a phase space model.

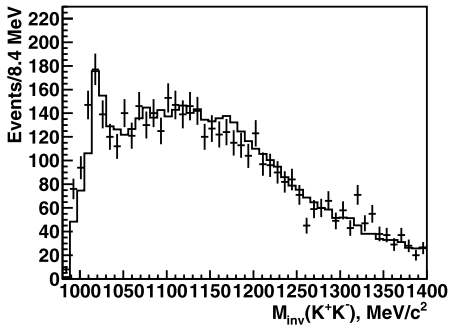

Fig. 10. K^+K^- invariant mass for data (points) and MC simulation (histogram) at $E_{\text{c.m.}} = 1950$ MeV.

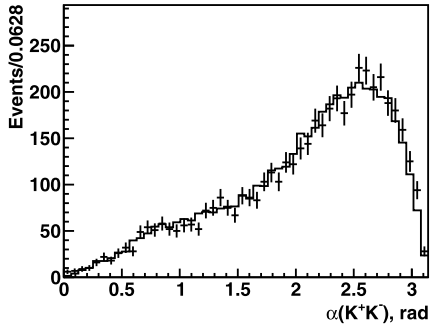

Fig. 11. The angle between K^+ and K^- for data (points) and MC simulation (histogram) at $E_{\text{c.m.}} = 1950$ MeV.

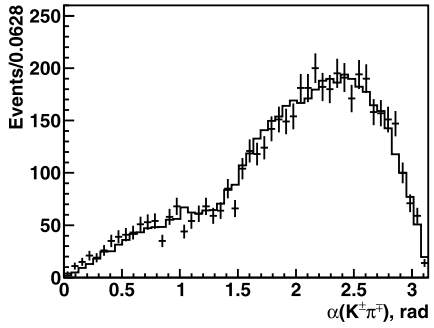

Fig. 12. The angle between $K^\pm$ and $\pi^\mp$ for data (points) and MC simulation (histogram) at $E_{\text{c.m.}} = 1950$ MeV.

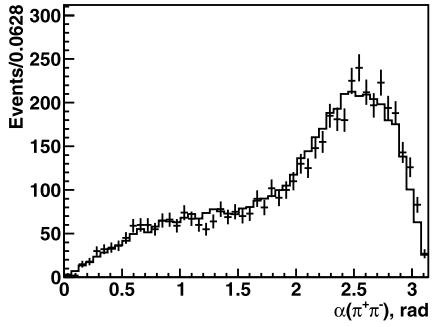

Fig. 13. The angle between π^+ and π^- for data (points) and MC simulation (histogram) at $E_{\text{c.m.}} = 1950$ MeV.

Since events with a missing track are mostly due to the limited DC acceptance, the ratio of the number of three-track and four-track events $R_{3/4}$ is sensitive to the polar-angle distributions, and provides an additional test of the production mechanism used in the MC simulation. Fig. 15 shows $R_{3/4}$ for missing pions (circles) and missing kaons (squares) in comparison with the corresponding simulated values shown by the smooth lines. We observe good agreement of the data and simulation and use this comparison to estimate systematic uncertainties on the detection efficiency discussed below.

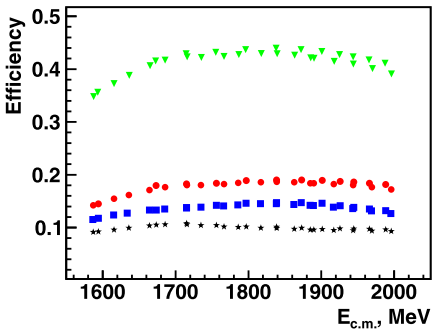

Fig. 14. Detection efficiency for four-track events (circles), events with a missing pion (stars), events with a missing kaon (squares) and total detection efficiency (triangles) vs c.m. energy.

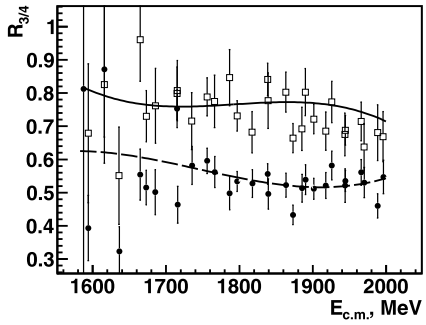

Fig. 15. The ratio of three- and four-track events, $R_{3/4}$, for a missing pion (circles) and a missing kaon (squares). The lines show corresponding simulated values.

Three-track events with a missing pion or kaon expected in the DC acceptance are used to estimate the single-track DC reconstruction efficiency for data and MC simulation. It is calculated as $\varepsilon_{1tr} = 2/(2 + R_{3/4})$, and we obtain $\varepsilon^{\text{exp}}_{1tr\ K} = 0.855 \pm 0.005$ ($\varepsilon^{\text{MC}}_{1tr\ K} = 0.862 \pm 0.005$) and $\varepsilon^{\text{exp}}_{1tr\ \pi} = 0.95 \pm 0.01$ ($\varepsilon^{\text{MC}}_{1tr\ \pi} = 0.955 \pm 0.005$) averaged over the c.m. energy range 1600–2000 MeV for kaons and pions, respectively.

Using these values we calculate the corrections to the number of three- and four-track experimental events, ξ_{4tr} and ξ_{3tr}:

$$\xi_{4tr} = \frac{(\varepsilon^{\text{exp}}_{1tr\ K})^2(\varepsilon^{\text{exp}}_{1tr\ \pi})^2}{(\varepsilon^{\text{MC}}_{1tr\ K})^2(\varepsilon^{\text{MC}}_{1tr\ \pi})^2},$$

$$\xi^{\pi}_{3tr} = \frac{(\varepsilon^{\text{exp}}_{1tr\ K})^2\varepsilon^{\text{exp}}_{1tr\ \pi}(1-\varepsilon^{\text{exp}}_{1tr\ \pi})}{(\varepsilon^{\text{MC}}_{1tr\ K})^2\varepsilon^{\text{MC}}_{1tr\ \pi}(1-\varepsilon^{\text{MC}}_{1tr\ \pi})},$$

$$\xi^{K}_{3tr} = \frac{(\varepsilon^{\text{exp}}_{1tr\ \pi})^2\varepsilon^{\text{exp}}_{1tr\ K}(1-\varepsilon^{\text{exp}}_{1tr\ K})}{(\varepsilon^{\text{MC}}_{1tr\ \pi})^2\varepsilon^{\text{MC}}_{1tr\ K}(1-\varepsilon^{\text{MC}}_{1tr\ K})}.$$

These corrections depend on conditions used to determine "good" tracks, and their values vary in the 0.95–1.05 range when we study systematic uncertainties (see below). For selected "good" tracks our simulation describes well the DC detection efficiency and corrections are about unity.

Fig. 16 presents the polar angle distribution for three-track events after background subtraction. The points correspond to experimental data, the open histogram is for simulation of tracks

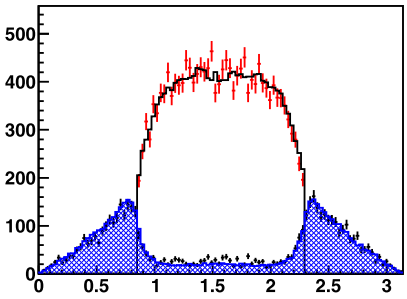

Fig. 16. The polar angle of kaon or pion. Points correspond to experimental data, histogram — simulation. The open region corresponds to the polar angle of detected particles, shaded — polar angle of the particles that were not detected.

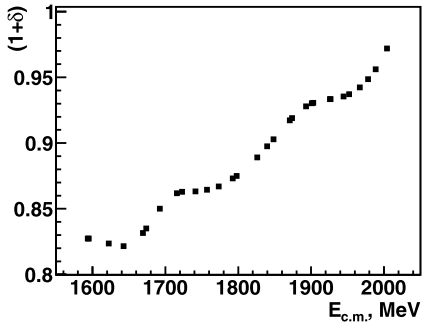

Fig. 17. A radiative correction versus c.m. energy.

detected in DC, and the shaded histogram shows the distribution for the expected direction of missing particles. The simulation describes our data well.

6. Cross section calculation

At each energy point the Born cross section for the process $e^+e^- \to K^+K^-\pi^+\pi^-$ is calculated as a weighted average of the cross sections for three different data sets:

$$\sigma_{4tr} = \frac{N_{4tr}}{\epsilon_{4tr} L_{\rm int}(1+\delta)\xi_{4tr}},$$

$$\sigma_{3tr\ K} = \frac{N_{3tr\ K}}{\epsilon_{3tr\ K} L_{\rm int}(1+\delta)\xi_{3tr\ K}},$$

and

$$\sigma_{3tr\ \pi} = \frac{N_{3tr\ \pi}}{\epsilon_{3tr\ \pi} L_{\rm int}(1+\delta)\xi_{3tr\ \pi}}$$

for four- and three-track events, where $L_{\rm int}$ is the integrated luminosity, $(1+\delta)$ is the radiative correction, ϵ_{4tr} and $\epsilon_{3tr\ K,\pi}$ are the detection efficiencies from simulation, ξ_{4tr} and $\xi_{3tr\ K,\pi}$ are corrections for the data–MC difference in the DC track reconstruction efficiencies.

The radiative correction shown in Fig. 17 is calculated according to [12,18], using our cross section data and an iteration procedure.

The obtained cross section is presented in Fig. 18 as a function of c.m. energy. Our result agrees with the previous measurement performed by the BaBar Collaboration [6] and has comparable or better statistical precision.

The integrated luminosity, the number of four- and three-track events, detection efficiency, radiative correction and obtained cross section for each energy point are listed in Table 1. Only statistical errors are shown.

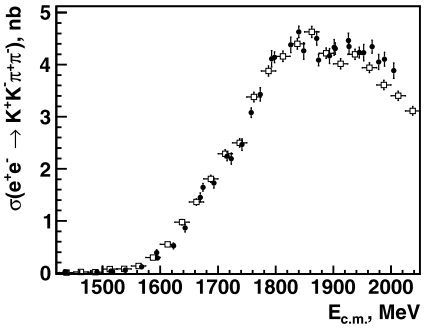

Fig. 18. The cross section of the process $e^+e^- \to K^+K^-\pi^+\pi^-$ obtained with the CMD-3 detector (dark circles) in comparison with the BaBar measurement (open circles).

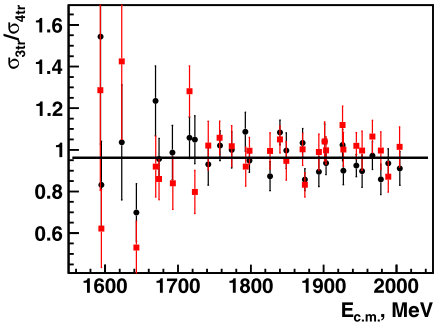

Fig. 19. The ratio of three-track and four-track cross sections. The line is an approximation.

7. Systematic errors

The following main sources of systematic uncertainties are considered:

- The uncertainty on the determination of the integrated luminosity is 1% [13];
- A systematic error due to the K/π separation is estimated to be 0.5%;
- Using the ratio of the cross section values obtained for the 2011 and 2012 runs we estimate a systematic uncertainty associated with overall detector operation as 1.2 %;
- The accuracy of background subtraction for three-track events is studied by the variation of the fit range and is estimated as 1.5%;
- A systematic error due to the selection criteria is studied by varying the "good" track definition and is estimated to be 2.6%;
- The model dependence uncertainty of 5% is conservatively estimated by varying the polar angle selection, and by comparison of the cross sections for four- and three-track events shown in Fig. 19. The mean value of the ratio of such events is 0.960 ± 0.024.

The above systematic uncertainties summed in quadrature give an overall systematic error of 6.1%.

An additional systematic uncertainty is related to the accuracy of c.m. energy determination, which is about 6 MeV and 2 MeV for the 2011 and 2012 runs, respectively. It leads to an energy-dependent uncertainty of about 10% at $E_{\rm c.m.} = 1500$–1600 MeV linearly decreasing to 1% at $E_{\rm c.m.} = 1800$ MeV. In the energy range $E_{\rm c.m.} = 1800$–2000 MeV this uncertainty is less than 1%. The c.m. energy uncertainties are listed in Table 1.

8. Conclusion

The total cross section of the process $e^+e^- \to K^+K^-\pi^+\pi^-$ has been measured using 23 pb^{-1} of an integrated luminosity collected with the CMD-3 detector at the VEPP-2000 collider in the 1500–2000 MeV c.m. energy range. Our results agree with the previous measurements and have comparable or better statistical precision. This final state exhibits complex resonant substructures. Our tentative study of dynamics shows the following major intermediate mechanisms: $e^+e^- \to (K_1(1270)K)_{\text{S-wave}} \to (K^*\pi)_{\text{S-wave}}K$, $e^+e^- \to (K_1(1400)K)_{\text{S-wave}} \to (K^*\pi)_{\text{S-wave}}K$, $e^+e^- \to (K_1(1270)K)_{\text{S-wave}} \to (\rho K)_{\text{S-wave}}K$, $e^+e^- \to f_0(980)\phi$, $e^+e^- \to f_0(500)\phi$ and $e^+e^- \to \rho(KK)_{\text{S-wave}}$. Simulation based on these models is in good agreement with the experimental data and allows one to measure the total cross section with a systematic uncertainty falling from 11.7% at 1500–1600 MeV to 6.1% above 1800 MeV. After VEPP-2000 upgrade it will be possible to perform a more detailed analysis of dynamics using higher statistics and various charge combinations of the $K\bar{K}\pi\pi$ final state. We also plan to improve K/π separation by using additionally ionization losses in the xenon barrel calorimeter.

Acknowledgements

This work is supported in part by the RFBR grants 13-02-00215, 13-02-01134, 14-02-31275, 14-02-00047, 14-02-91332, 14-02-31478, 15-02-05674 and the DFG grant HA 1457/9-1. Investigation of the ionization losses in the LXe calorimeter (Section 3) has been supported by Russian Science Foundation (Project 14-50-00080).

References

[1] K. Hagiwara, R. Liao, A.D. Martin, D. Nomura, T. Teubner, J. Phys. G 38 (2011) 085003;
M. Davier, A. Hoecker, B. Malaescu, Z. Zhang, Eur. Phys. J. C 71 (2011) 1515;
M. Davier, A. Hoecker, B. Malaescu, Z. Zhang, Eur. Phys. J. C 72 (2012) 1874.
[2] G.W. Bennett, et al., Muon g-2 Collaboration, Phys. Rev. D 73 (2006) 072003.
[3] A. Cordier, et al., DM1 Collaboration, Phys. Lett. B 110 (1982) 335.
[4] D. Bisello, et al., DM2 Collaboration, Nucl. Phys. B, Proc. Suppl. 21 (1991) 111;
M.R. Whalley, J. Phys. G 29 (2003) A1.
[5] B. Aubert, et al., BaBar Collaboration, Phys. Rev. D 76 (2007) 012008.
[6] J.P. Lees, et al., BaBar Collaboration, Phys. Rev. D 86 (2012) 012008.
[7] C.P. Shen, et al., Belle Collaboration, Phys. Rev. D 80 (2009) 031101.
[8] D.E. Berkaev, et al., JETP 113 (2011) 213.
[9] B.I. Khazin, et al., CMD-3 Collaboration, Nucl. Phys. B, Proc. Suppl. 181–182 (2008) 376.
[10] V.M. Aulchenko, et al., J. Instrum. 10 (2015) P10006.
[11] S. Agostinelli, et al., GEANT4 Collaboration, Nucl. Instrum. Methods A 506 (2003) 250.
[12] E.A. Kuraev, V.S. Fadin, Sov. J. Nucl. Phys. 41 (1985) 466.
[13] R.R. Akhmetshin, et al., CMD-3 Collaboration, Nucl. Phys. B, Proc. Suppl. 225–227 (2012) 69.
[14] E.V. Abakumova, et al., Phys. Rev. Lett. 110 (2013) 140402.
[15] E.V. Abakumova, et al., J. Instrum. 10 (2015) T09001.
[16] R.R. Akhmetshin, et al., CMD-3 Collaboration, arXiv:1507.08013, Phys. Lett. B (2016), in press.
[17] H. Czyż, et al., arXiv:1312.0454.
[18] S. Actis, et al., Eur. Phys. J. C 66 (2010) 585.